Biosensors and Bioelectronics 209 (2022) 114239

Contents lists available at ScienceDirect

Biosensors and Bioelectronics

journal homepage: www.elsevier.com/locate/bios

Hollow covalent organic framework-sheltering CRISPR/Cas12a as an in-vivo nanosensor for ATP imaging

Yongchun Pan [a,b], Xiaowei Luan [a], Fei Zeng [a], Qin Xu [a], Zekun Li [c], Yanfeng Gao [a], Xinli Liu [d], Xueqing Li [a], Xin Han [c,**], Jianliang Shen [b,e,***], Yujun Song [a,b,*]

[a] College of Engineering and Applied Sciences, State Key Laboratory of Analytical Chemistry for Life Science, Nanjing University, Nanjing, 210023, China
[b] Engineering Research Center of Clinical Functional Materials and Diagnosis & Treatment Devices of Zhejiang Province, Wenzhou Institute, University of Chinese Academy of Sciences, Wenzhou, 325024, China
[c] School of Medicine & Holistic Integrative Medicine, Jiangsu Collaborative Innovation Center of Chinese Medicinal Resources Industrialization, Nanjing University of Chinese Medicine, Nanjing, 210023, China
[d] Life Sciences Institute, Guangxi Key Laboratory of Early Prevention and Treatment for Regional High Frequency Tumor, Guangxi Medical University, Nanning, 530021, China
[e] School of Ophthalmology & Optometry, School of Biomedical Engineering, Wenzhou Medical University, Wenzhou, 325035, China

ARTICLE INFO

Keywords:
Trans-cleavage activity
Aptamers
Small molecule diagnostics
Porous nanomaterials

ABSTRACT

In addition to applications in genome editing, clustered regularly interspaced short palindromic repeats (CRISPR) have recently been engineered for medical diagnostics based on their trans-cleavage activity owing to their high base resolution and isothermal signal amplification. However, trans-cleavage activity is too fragile to be applied in vivo. Herein, we introduce a hollow covalent organic framework (COF)-sheltering CRISPR/aptamer-based sensor (h-CCS) for ATP imaging in living animals. The CRISPR/aptamer-based complex is comprised of the CRISPR-Cas12a system, fluorophore quencher-labeled single-stranded DNA substrate (ssDNA-FQ), and a DNA activator that pre-hybridizes with ATP aptamer to prevent the trans-cleavage activity of the Cas12a system in the absence of ATP. After being encapsulated in a hollow COF, the constructed nanoreactor is highly robust and can be lit up by ATP for in vivo imaging. Considering the unique properties of h-CCS, this strategy offers great potential to broaden applications of not only CRISPR-Cas systems but also other proteins in porous matrixes for clinical diagnostics, medical research, and biomimetic nanodevices.

1. Introduction

Recent advances toward clustered regularly interspaced short palindromic repeats (CRISPR) and CRISPR-associated proteins (Cas) have opened a new window onto genome editing for extensive applications, especially in the life sciences (Cong et al., 2013; Doudna, 2020; Jinek et al., 2012; Li et al., 2021; Pan et al., 2019). Additionally, the recent discovery of the non-specific nucleic acid cleavage (collateral cleavage or *trans*-cleavage) activity of the Cas14, Cas13, and Cas12 effectors has ignited growing attention in medical diagnostics based on CRISPR due to its high sensitivity, practical economy, and isothermal signal amplification (Chen et al., 2018; Dai et al., 2020; Gootenberg et al., 2018; Harrington et al., 2018; Xiong et al., 2020). Up to date, seminal works with such CRISPR systems have contributed to the development of DNA, RNA, protein, ATP, and ion sensors (Dai et al., 2019; Xiong et al., 2020; Zhao et al., 2021b; Zhou et al., 2020). However, the applications of *trans*-cleavage activity in complex intracellular environments remain vague and in the exploration and practice phases (Wang et al., 2019).

Compartmentalization of biomacromolecules and reactions in confined locations known as organelles for complex metabolic reactions features living systems (Bhattacharya et al., 2020; Hyman et al., 2014; Li et al., 2020a). Such spatial organizations guarantee better biochemical functions by controlling reactant accessibility, providing physical

* Corresponding author. College of Engineering and Applied Sciences, State Key Laboratory of Analytical Chemistry for Life Science, Nanjing University, Nanjing, 210023, China.
** Corresponding author.
*** Corresponding author. Engineering Research Center of Clinical Functional Materials and Diagnosis & Treatment Devices of Zhejiang Province, Wenzhou Institute, University of Chinese Academy of Sciences, Wenzhou, 325024, China.
E-mail addresses: xhan0220@njucm.edu.cn (X. Han), shenjl@wiucas.ac.cn (J. Shen), ysong@nju.edu.cn (Y. Song).

https://doi.org/10.1016/j.bios.2022.114239
Received 22 January 2022; Received in revised form 24 March 2022; Accepted 31 March 2022
Available online 3 April 2022
0956-5663/© 2022 Elsevier B.V. All rights reserved.

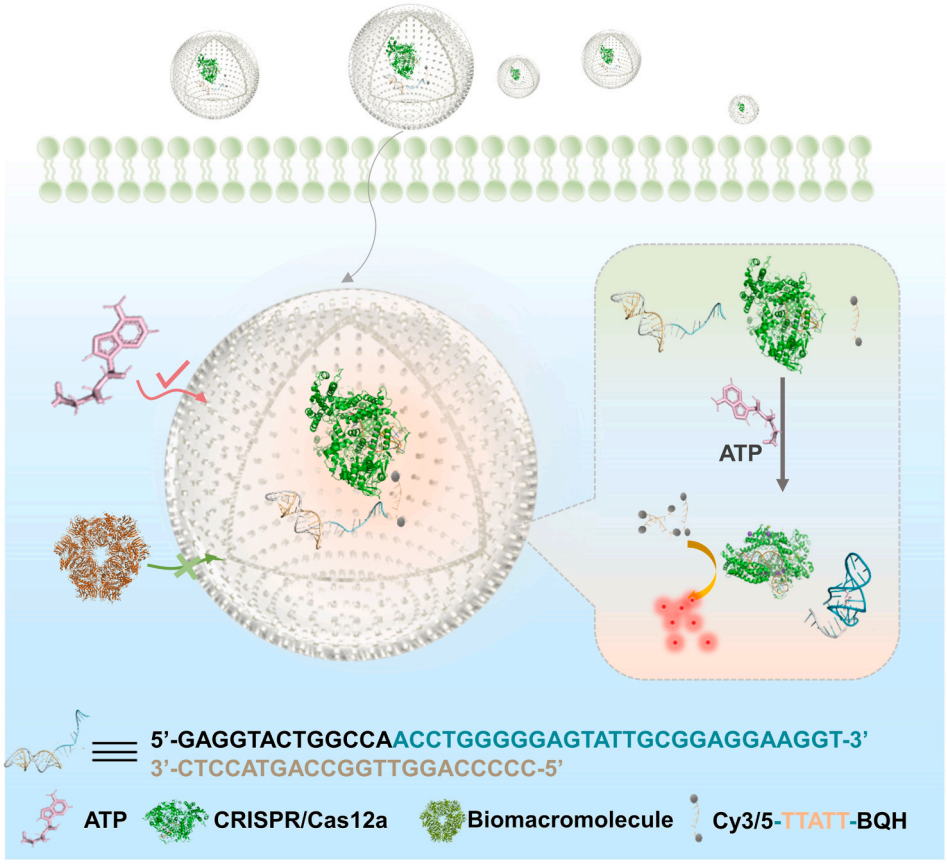


Fig. 1. Schematic illustration of a hollow COF-sheltering CRISPR/aptamer-based sensor triggered by ATP for tumor imaging.

protection against external disturbance, and allowing considerable freedom for macromolecules (Kiekebusch and Thanbichler, 2014). Inspired by these findings, substantial pioneering studies have been proposed for the development of organelle-like hollow nano/-microstructures, including polymer assemblies and hollow mesoporous silica nanoparticles (Feng et al., 2016; Jo et al., 2020; Lee et al., 2018; Yu et al., 2018). Recently, metal-organic frameworks (MOFs) have emerged as suitable scaffolds for protein support owing to their unique intrinsic properties, including high specific surface areas, adaptable structures, and customizable functionality (Della Rocca et al., 2011; Li et al., 2020b; Zhang et al., 2018b). However, protein@MOF can be readily digested by abundant biomarkers, such as H^+ and ATP, in the tumor microenvironment and lose the protective effect of the protein (Liang et al., 2015; Yang et al., 2019). In contrast, another porous material, covalent organic framework (COF), demonstrated higher stability, but its harsh synthetic conditions and potential effect on macromolecular conformation by residual chemical bonds of COFs are obstructing the application of COFs in encapsulating biomacromolecules via a "one-pot" strategy (Geng et al., 2020; Li et al., 2020a; Sun et al., 2018). Therefore, fabricating a COF-like robust but MOF-like biomacromolecular-friendly artificial organelle to confine proteins to exert their effect in cells remains challenging.

Beyond providing energy, ATP is also involved in a series of physiological and pathological processes, including cell growth, inflammation, and transplant immunity, as a signaling molecule (Idzko et al., 2014; Zhao et al., 2021a). Such clear significance calls for accuracy in vivo detection methods. At present, luciferase and its substrate luciferin are widely employed to monitor the level via an ATP-dependent luminescent reaction, but the strong dependence on the substrates (e.g., oxygen, exogenously supplied luciferin) and various interferences between the sample matrix and cellular factors limit its application (Morciano et al., 2017). Although demonstrated appealing real-time imaging features, recent genetically encoded fluorescent ATP sensors, such as iATPSnFRs and ATeam, are limited by low signal levels or indirect ATP responses (Berg et al., 2009; Imamura et al., 2009; Lobas et al., 2019). Hence, further explorations remain required for flexible and sensitive in-vivo ATP imaging.

Herein, we prepared a COF-derived nanoreactor to package the CRISPR-Cas12a system for ATP imaging in vivo (Fig. 1). The CRISPR/aptamer-based sensor (CS) was first designed to detect ATP and then encapsulated *in situ* within amorphous zeolitic imidazolate framework (ZIF)-8 (CS@a-ZIF-8), which served as a template for the growth of CS@a-ZIF-8@COF core-shell structures. Finally, the a-ZIF-8 core was etched away to liberate the sensor within the hollow COF capsule (Fig. 2A). This commodious environment provided the enzyme with conformational freedom and alienated Cas12a from complex substrates in the biological environment. With the hollow COF, we have achieved an ATP-fuelled *trans*-cleavage activity-based CRISPR platform in vivo.

2. Experimental section

2.1. Syntheses of h-CCS

First, CS, Zn^{2+}, and 2-methylimidazole were mixed to synthesize CS@a-ZIF-8. After encapsulation, the resulting product was redispersed, and 4,4′-diaminobiphenyl and 2,4,6-trihydroxybenzene-1,3,5-tricarbaldehyde (21.0 mg/mL) were added to obtain CS@a-ZIF-8@COF. To obtain the hollow structure, acetic acid was used to etch ZIF-8 for the final h-CCS (see Supporting Information for details).

2.2. Cell imaging

For the microscopic study, cells were plated into 20-mm 4-chamber glass-bottom dishes (Cellvis, CA, USA) overnight to allow their

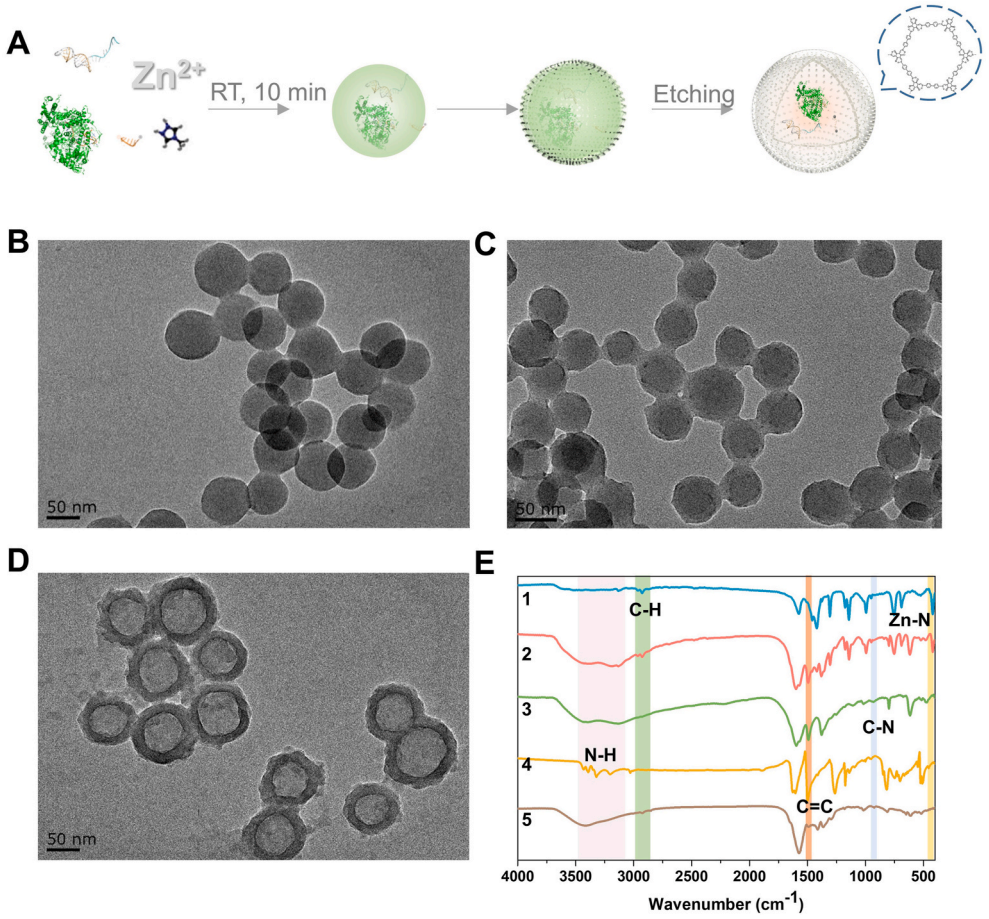


Fig. 2. Construction of h-CCS. (A) Synthetic route to h-CCS; TEM images of (B) CS@a-ZIF-8; (C) CS@a-ZIF-8@COF; (D) h-CCS. (E) FT-IR spectra of 1: a-ZIF-8, 2:a-ZIF-8@COF, 3: hollow COF, 4: benzidine, 5: 2,4,6-triamino-1,3,5-trioxy-benzol.

attachment to the glass bottom. Before incubation with h-CCS, the cells were pretreated with or without 300 nM oligomycin and 5 mM Ca^{2+} for 2 h. After that, the cells were washed three times with PBS buffer and then imaged using laser scanning confocal microscopy (Leica TCS SP5, Germany). The images were collected at 550–580 nm upon excitation at 532 nm.

2.3. *In vivo imaging*

Animal procedures were performed according to the guidelines of Nanjing University Medical School. Female BALB/c nude mice (16–18 g) were subcutaneously injected with freshly harvested A549 cells at the back of the mouse. After the tumor size reached 100–200 mm^2, the nude mice were arbitrarily divided into 3 groups for treatment with COF-Cy5, mut-CCS, and h-CCS. The mice were intratumorally or intravenously injected with COF-Cy3, mut-CCS, and h-CCS (Cy5-DNA probe dose of 25 nmol/kg). Whole-body fluorescence imaging of A549 tumor-bearing mice after different treatments was performed using an IVIS system over time. Mice were anesthetized after 12 h of treatment, and the tumors and major organs were harvested and subjected to ex vivo imaging. Regions of interest were circled in the tumors and analyzed using Living Image Software.

3. Results and discussion

As a proof of concept for the ATP-sensitive CRISPR-Cas12a system, the ATP aptamer was designed to hybridize with the DNA activator to inhibit trans-cleavage activity in the absence of ATP (see Fig. S1A). Specifically, the sensor is composed of CRISPR-Cas12a, ATP aptamer-hybridized activator, and a single-stranded DNA (ssDNA) reporter labeled with a fluorophore and quencher pair (denoted as ssDNA-FQ). Once ATP occurs, the aptamer experiences a structural switch (or conformational change) to bind ATP, leading to a weakened interaction with the DNA activator and reducing the melting temperature of the remaining nucleotides and thereby releasing the DNA activator to trigger the *trans*-cleavage activity of CRISPR-Cas12a. To further verify the validity of CS, we recorded the fluorescence responses of CS to ATP at varying concentrations. Since the ssDNA-FQ reporters could be cleaved by activated Cas12a, fluorescence was observed, and the signals were proportional to the ATP dosage (Figs. S1B and C). After 30 min of different ATP processing, we measured the fluorescence intensity and found that the fluorescence intensity at a low concentration of ATP (1.0 μM) obtained an approximately 3-fold increase compared with that treated without ATP, which demonstrates the good detection performance of this sensor. Besides, the results provided a linear range from 0.1 to 1.0 μM for ATP detection (Fig. S1C). To evaluate the selectivity of CS, we investigated the fluorescence responses toward other nucleotide-triphosphate analogs, i.e., GTP, CTP, and UTP. As shown in Fig. S1D, these competing nucleotide-triphosphate analogs initiated no obvious changes in fluorescence intensity at a concentration of 1.0 mM, while the signal after treatment with 20 μM ATP received more than 6-fold signal enhancement, indicating the high selectivity of the ATP aptamer for the CRISPR/aptamer-based sensor.

Subsequently, we packaged the aforementioned CS in a COF-sheltering capsule. As shown in Fig. 2A, a three-step procedure was proposed to build the h-CCS: 1) encapsulating CS in a-ZIF-8 by mixing with 2-methylimidazole (40 mM) and zinc acetate (15 mM) (CS@a-ZIF-8); 2) coating with COF shell (CS@a-ZIF-8@COF); 3) hollowing ZIF-8 by

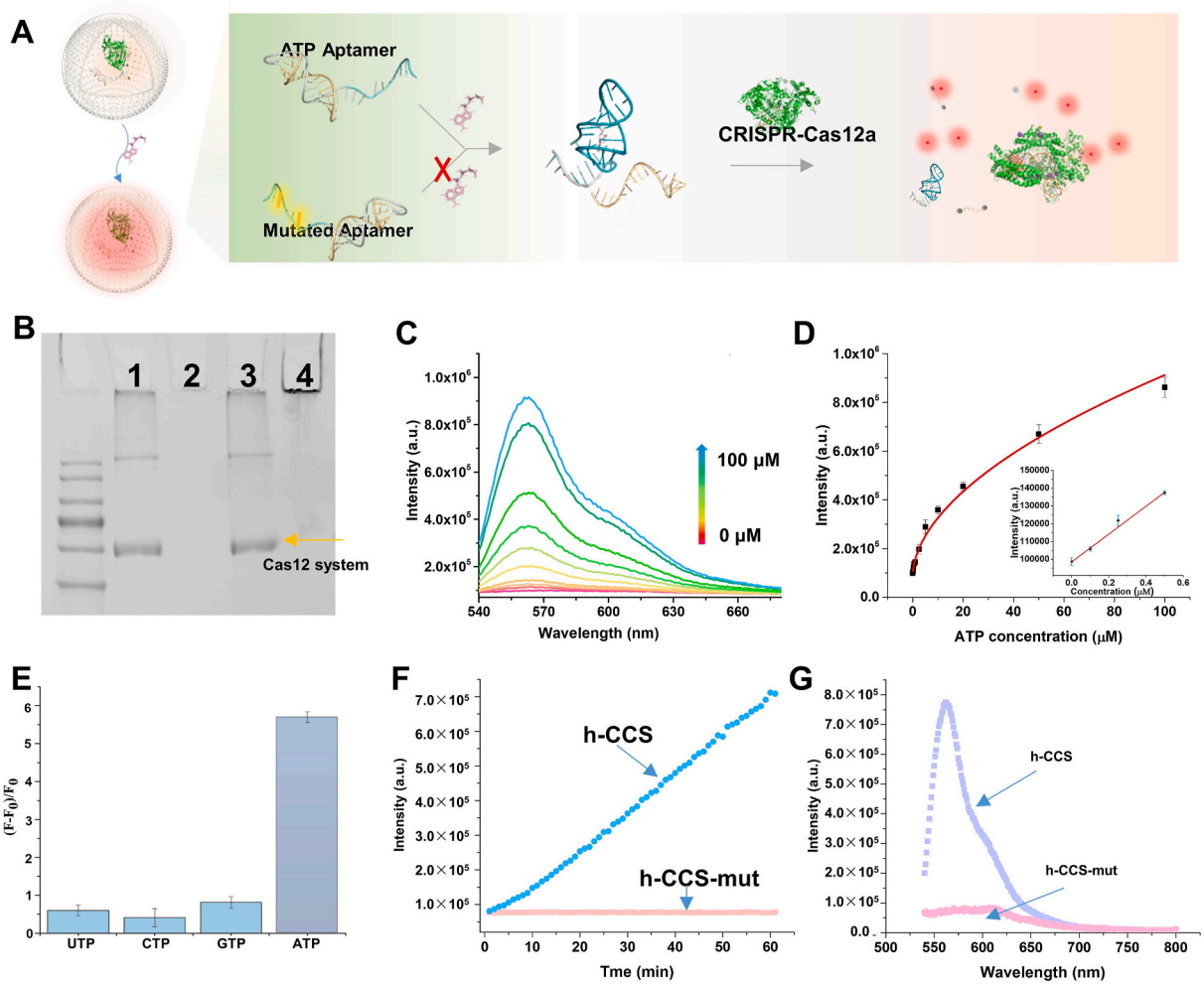


Fig. 3. The detection performance of h-CCS. (A) Schematic illustration of the working principle of CRISPR/aptamer-based ATP sensor; (B) Page gel electrophoresis for h-CCS (1: control, 2: supernatant, 3: CS@a-ZIF-8+H^+, 4: h-CCS+H^+); (C) Fluorescence responses of the h-CCS to ATP of varying concentrations from bottom to top: 0 (blank), 0.1, 0.25, 1.0, 2.5, 5.0, 10, 25, 50 and 100 μM; (D) Fluorescence titration curve of h-CCS for ATP; (E) Specificity evaluation of h-CCS for ATP detection; the concentrations of ATP was set at 20 μM, while other nucleotide-triphosphate analogs was 1.0 mM (F denotes fluorescence intensity, while F_0 denotes initial fluorescence intensity). (F) Kinetic curves and (G) fluorescence spectra of h-CCS and h–CCS–mut in response to 5 mM ATP. Data represent the mean ± s.d., n = 3, three technical replicates.

acid etching. The resulting transmission electron microscopy (TEM) images and DLS analyses demonstrated that loading CS barely influenced the morphology of a-ZIF-8, except with a larger size (Figs. S2, S3, 2B, C, and D). The zeta potential analysis and FT-IR spectra showed the reaction process (Figs. 2E and S4). Besides, powder X-ray diffraction (PXRD) patterns (Fig. S5) implied the amorphous structures of our system, which was consistent with a previous report (Wu et al., 2019). In addition, we noticed that the pore diameter of the COF is about 4.0 nm (Fig. S6), which was small enough for the travel restrictions of most biomolecules. To directly confirm the successful encapsulation of CS, energy dispersive spectroscopy (EDS) elemental mapping was performed. The distributions of P from DNA and sgRNA and S from protein illustrated that CS was successfully retained in hollow COF (Fig. S7). We also used gel electrophoresis analysis to trace the Cas12a protein. After incubation with H^+, the CS@a-ZIF-8 group displayed clear Cas12a blotting, while no protein band appeared in the CS@a-ZIF-8@COF group (Fig. 3B), indicating that CS was loaded in ZIF-8 but hardly escaped from the COF-sheltering shell. For DNA encapsulation, we obtained similar results by detecting the fluorescence signals in h-CCS, where the aptamer was labeled with carboxyfluorescein (FAM) and 5-nt ssDNA was labeled with Cy3 (Fig. S8).

Next, the ATP-response performance of h-CCS was evaluated. We found that the COF shelter demonstrated no obvious fluorescence and merely influenced the Cy3 signal (Fig. S9). Based on that, a positive correlation was obtained for fluorescent intensity peaks at 566 nm to the ATP concentrations in the range from 0 to 100 μM, and the limit of detection (LOD) was calculated as 45 nM (Fig. 3C, and D). To validate the specificity of h-CCS for ATP analysis, the fluorescence responses toward other analogs were examined as well, and only ATP induced a significant fluorescence enhancement (Fig. 3E, Fig. S10). To further confirm ATP responsiveness, a mutated DNA strand, which is insensitive to ATP (Zhao et al., 2018), was employed to replace the above ATP aptamer in CS. The results displayed no obvious change in the mutated system after the addition of ATP, as expected (Fig. 3F–G). Besides, we also verified the feasibility of the sensor in a serum-containing environment. As shown in Fig. S11, the recovery rates ranged from 96.76% to 109.9%, indicating the high reliability of our sensor.

Direct delivery of biomacromolecules remains a challenge; thus, we studied the internalization performance of a hollow FAM-labeled CRISPR platform in human non-small lung cancer cells (A549 cells). As shown in Fig. S12, no significant green fluorescence was observed when treated with the free FAM-labeled CRISPR sensor, suggesting inefficient cellular uptake of CRISPR-Cas12a. In contrast, hollow COFs could facilitate internalization of the CRISPR sensor, contributing to an

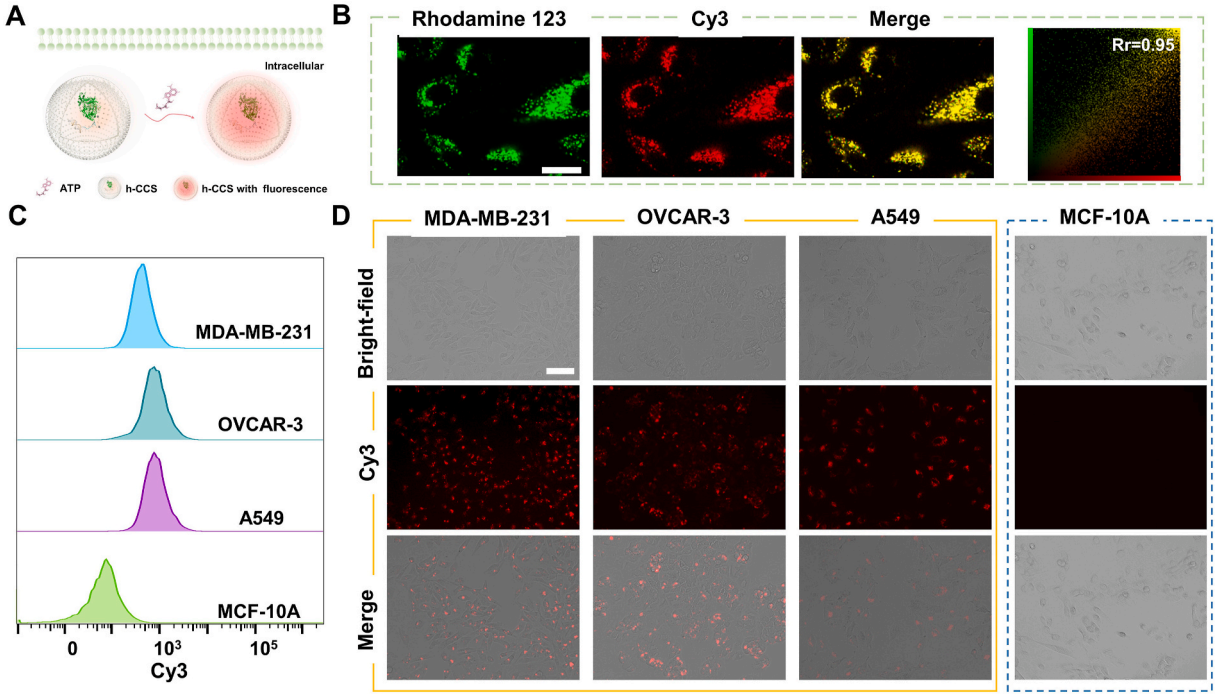


Fig. 4. ATP-fuelled h-CCS in living cells. (A) Schematic illustration of intracellular ATP-activated h-CCS. (B) Confocal fluorescence images of A549 cells co-stained with Cy3-labeled h-CCS and Rhodamine 123 and the red-green colocalization plot with Pearson's correlation Rr = 0.95, scale bar: 10 μm. (C) Flow cytometry results, and (D) images of different cell lines incubated with h-CCS for 4 h at 37 °C. Scale bar: 25 μm. MDA-MB-231, OVCAR-3, and A549 are cancer cell lines, while MCF-10A is a healthy cell line. For the representativeness of qualitative images, at least three experiments were carried out in duplicate.

obvious fluorescence signal in the cells. We next investigated the distribution of h-CCS inside cells (Fig. 4 and Fig. S13). The images showed that the fluorescence signal of h-CCS preferred to co-localize with MitoTracker (Rhodamine 123) instead of LysoTracker, indicating that h-CCS was probably transported to mitochondrial compartments. This could be attributed to the positive surface charges of h-CCS that facilitate the accumulation of h-CCS within mitochondria with a negatively charged inner membrane.

Apart from the enhanced internalization of the CRISPR sensor, the COF shelter also provided a compartmentalized bioenvironmental to protect the *trans*-cleavage of the sensor (Fig. S14). To investigate the generality of the protection effect, a DNA-based Ag^+ sensor and glucose oxidase (GOx) were encapsulated in hollow COFs. As shown in Fig. S15, in the presence of both Ag^+ and DNase I, the structure of the DNAzyme sensor was destroyed, leading to cleaved fragment release and fluorescence recovery. In contrast, the hollow COF protected the DNAzyme from DNase I but allowed access for Ag^+ (Fig. S15C). Similarly, GOx in the hollow COF withstood the hydrolyzation of proteinase K and displayed good biological activities (Fig. S16), indicating a selective permeability of hollow COF for glucose accessibility while keeping the enzymes inside. Due to the lower extracellular pH of the tumor microenvironment than that of normal cells, we performed a comparison of the internalization of the two composites (GOx@aZIF and GOx@COF) in acidic and basic environments to further investigate the robustness of the hollow COF. As shown in Fig. S16, ZIF-8 dissociated in an acidic environment, which resulted in the relatively lower transfection efficiency of GOx than that in alkaline solution; therefore, a higher fluorescence signal was obtained in an alkaline environment after 2 h of incubation. In contrast, there was no significant difference in the alkaline and acidic environments for GOx@COF. Overall, this developed method can be employed to protect various enzymes from macromolecular inhibitors and expand enzyme utilization in complex environments.

We then evaluated the ATP-responsive performance of h-CCS in living cells. A CCK-8 assay was first conducted to examine the cytotoxicity of h-CCS, and cell viabilities over 80% were obtained when the concentration was lower than 100 μg/mL (Fig. S17). Hence, the following imaging experiments were set at a concentration of 50 μg/mL. As shown in Fig. S18, the Cy3 fluorescence in cells after incubation with h-CCS gradually increased with time. As a control, neither the COF nor the free CRISPR-Cas12a system initiated significant red fluorescence after 8 h of treatment. To determine whether the signal was dependent on intracellular ATP, we employed different drug stimulations with no influence on Cas12a to regulate the endogenous ATP level (Fig. S19). Fig. S20 shows that the treatment of A549 cells with oligomycin (a known inhibitor of ATP (Gong et al., 2006; Zhang et al., 2018a)) led to a significant decrease in red fluorescence compared to that without oligomycin treatment. In contrast, Ca^{2+} (a stimulation that promotes intracellular ATP production (Deng et al., 2017; Zamaraeva et al., 2007)) incubation contributed to an enhancement of the Cy3 fluorescence signal (Fig. S20). Furthermore, we obtained similar results by examining the whole cell population using flow cytometry (Fig. S20). To further eliminate the possibility of artifacts in living cells, h–CCS–mut was incubated with cancer cells, and weaker fluorescence was also observed in the subsequent cell experiment, indicating ATP sensing specificity (Fig. S21).

Due to the high concentration of ATP (5–10 mM) in cancer cells, we investigated whether h-CCS can specifically trace cancer cells from healthy cells. As anticipated, MDA-MB-231 human breast cancer cells displayed a red fluorescence signal from the cleavage of ssDNA-FQ by Cas12a after incubation with h-CCS (Fig. 4). Additionally, clear fluorescence in the Cy3 channel emission was also observed in the cytoplasm of other cancer cell lines (Fig. 4). In contrast, healthy cells, a human breast epithelial cell line (MCF-10A) with a low ATP concentration, demonstrated negligible fluorescence responses.

Finally, we explored the application of h-CCS for ATP imaging in vivo. The h-CCS was subcutaneously injected into A549 tumor-bearing mice (the ssDNA reporter was labeled with Cy5 and a quencher pair), and fluorescence images were recorded using an in vivo imaging system (IVIS). As shown in Fig. S22A, an increase in fluorescence intensity at the

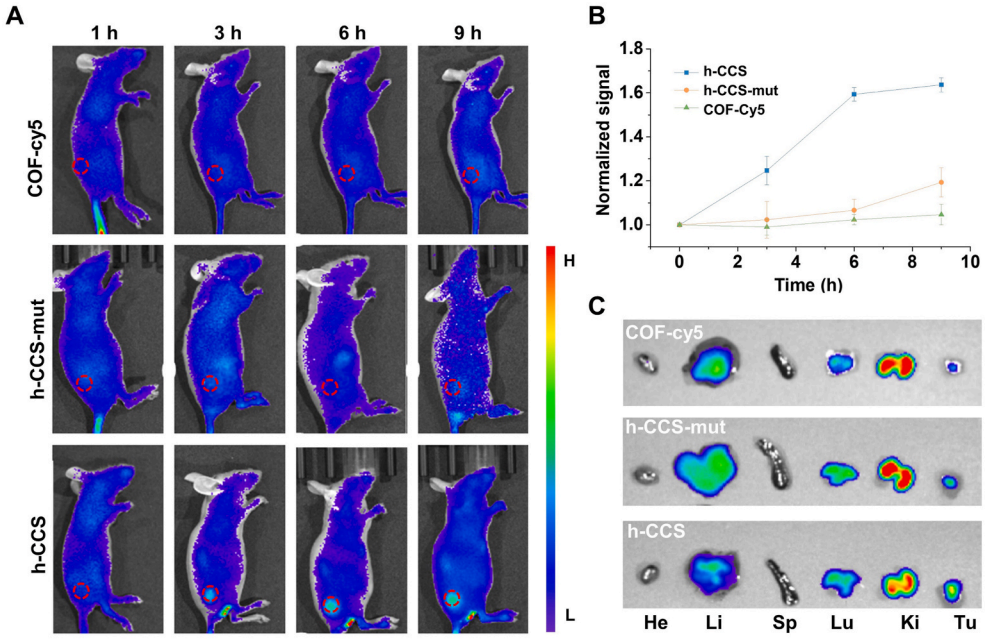


Fig. 5. In vivo ATP imaging via intravenous injection of h-CCS. (A) Whole-body fluorescence imaging of A549 tumor-bearing mice at different injection times. Tumor sites are indicated by red circles. (B) Fluorescence quantification of the tumor sites in red circles. (C) Ex vivo imaging of the major organs and tumors collected from mice 12 h after intravenous administration as indicated (He = heart; Li = liver; Sp = spleen; Lu = lung; Ki = kidney; Tu = tumor). Data represent the mean ± s.d., n = 5, five technical replicates.

tumor site as a function of time was observed by IVIS, and the signal plateau was reached at about 6 h. Quantitative analysis showed that h–CCS–treated mice demonstrated approximately 1.4- and 2.1-fold higher intratumoral Cy5 signals at 3 h and 6 h, respectively, than at 1 h (Fig. S22B). In contrast, no significant enhancement of fluorescence intensity at the tumor site was detected after injection of either h–CCS–mut or COF-Cy5 (Fig. S22), suggesting that the signal increase in the h-CCS group originated from ATP encouragement instead of COF itself or DNase in vivo. The ATP-activated nanoplatform was also tested in living mice via intravenous administration (i.v.), and we obtained similar results, as shown in Fig. 5. Besides, ex vivo imaging was performed by measuring the Cy5 fluorescence intensity in collected organs and tumors from the mice 12 h after injection of different drugs (Fig. 5C). The intratumoral fluorescent signal in the h-CCS group was higher than that in the h–CCS–mut and COF-Cy5 groups, while no distinct difference in Cy5 intensity in the main organs was observed for all groups. These results demonstrated that robust h-CCS was available for visualizing ATP in living mice.

4. Conclusion

In summary, we reported a hollow COF-shielding CRISPR/aptamer-based nanoreactor for in vivo ATP imaging. The nanoreactor demonstrated inherently high specificity assisted by ATP aptamer CRISPR-Cas recognition. In addition, the h-CCS with COF-shell for resisting external macromolecule disturbance exhibited high robustness to trace ATP even in the complex biological matrix, which endows the sensor with in vivo imaging features. Due to its high functional stability, readily available aptamer library for a wide range of targets, and desirable cell permeability, the nanoreactor holds enormous potential beyond imaging in a complicated biological environment. Indeed, this method is only available for small molecule detection at present. To expand the strategy for in vivo microRNA imaging, a suitable mesoporous material remains to be explored and conquered. Altogether, this design broadened the biomedical applications of CRISPR-Cas systems and inspired the further understanding of protein behavior in micro/nano environments for the fabrication of more ingenious biomimetic nanodevices and artificial cells.

CRediT authorship contribution statement

Yongchun Pan: Methodology, Validation, Formal analysis, Investigation, Data curation, Writing – original draft. **Xiaowei Luan:** Methodology, Writing – review & editing. **Fei Zeng:** Investigation. **Qin Xu:** Writing – review & editing. **Zekun Li:** Resources. **Yanfeng Gao:** Writing – review & editing. **Xinli Liu:** Resources. **Xueqing Li:** Resources. **Xin Han:** Project administration, Funding acquisition, Writing – review & editing. **Jianliang Shen:** Funding acquisition, Writing – review & editing. **Yujun Song:** Conceptualization, Supervision, Project administration, Funding acquisition, Writing – review & editing.

Declaration of competing interest

The authors declare that they have no known competing financial interests or personal relationships that could have appeared to influence the work reported in this paper.

Acknowledgements

This research was made possible as a result of a generous grant from the National Natural Science Foundation of China (21874066, and 81601632), the Key Research and Development Program of Jiangsu Province (BE2021373), the Natural Science Foundation of Jiangsu Province (BK20160616, and BK20200336), the Fundamental Research Funds for Central Universities, the Program for Innovative Talents and Entrepreneur in Jiangsu, Engineering Research Center of Clinical Functional Materials and Diagnosis & Treatment Devices of Zhejiang Province (WIUCASK20010), and Postgraduate Research & Practice Innovation Program of Jiangsu Province (KYCX20_0036).

Appendix A. Supplementary data

Supplementary data to this article can be found online at https://doi.org/10.1016/j.bios.2022.114239.

References

Berg, J., Hung, Y.P., Yellen, G., 2009. A genetically encoded fluorescent reporter of ATP: ADP ratio. Nat. Methods 6 (2), 161–166.

Bhattacharya, A., Niederholtmeyer, H., Podolsky, K.A., Bhattacharya, R., Song, J.-J., Brea, R.J., Tsai, C.-H., Sinha, S.K., Devaraj, N.K., 2020. Lipid sponge droplets as programmable synthetic organelles. Proc. Natl. Acad. Sci. Unit. States Am. 117 (31), 18206–18215.
Chen, J.S., Ma, E., Harrington, L.B., Da Costa, M., Tian, X., Palefsky, J.M., Doudna, J.A., 2018. CRISPR-Cas12a target binding unleashes indiscriminate single-stranded DNase activity. Science 360 (6387), 436–439.
Cong, L., Ran, F.A., Cox, D., Lin, S., Barretto, R., Habib, N., Hsu, P.D., Wu, X., Jiang, W., Marraffini, L.A., Zhang, F., 2013. Multiplex genome engineering using CRISPR/Cas systems. Science 339 (6121), 819–823.
Dai, Y., Somoza, R.A., Wang, L., Welter, J.F., Li, Y., Caplan, A.I., Liu, C.C., 2019. Exploring the trans-cleavage activity of CRISPR-Cas12a (cpf1) for the development of a Universal electrochemical biosensor. Angew. Chem. Int. Ed. 58 (48), 17399–17405.
Dai, Y., Wu, Y., Liu, G., Gooding, J.J., 2020. CRISPR mediated biosensing toward understanding cellular biology and point-of-care Diagnosis. Angew. Chem. Int. Ed. 59 (47), 20754–20766.
Della Rocca, J., Liu, D., Lin, W., 2011. Nanoscale metal–organic frameworks for biomedical imaging and drug delivery. Accounts Chem. Res. 44 (10), 957–968.
Deng, J., Wang, K., Wang, M., Yu, P., Mao, L., 2017. Mitochondria targeted nanoscale zeolitic imidazole framework-90 for ATP imaging in live cells. J. Am. Chem. Soc. 139 (16), 5877–5882.
Doudna, J.A., 2020. The promise and challenge of therapeutic genome editing. Nature 578 (7794), 229–236.
Feng, X., Jia, Y., Cai, P., Fei, J., Li, J., 2016. Coassembly of photosystem II and ATPase as artificial chloroplast for light-driven ATP synthesis. ACS Nano 10 (1), 556–561.
Geng, K., He, T., Liu, R., Dalapati, S., Tan, K.T., Li, Z., Tao, S., Gong, Y., Jiang, Q., Jiang, D., 2020. Covalent organic frameworks: design, synthesis, and functions. Chem. Rev. 120 (16), 8814–8933.
Gong, Y., Sohn, H., Xue, L., Firestone, G.L., Bjeldanes, L.F., 2006. 3,3'-Diindolylmethane is a novel mitochondrial H(+)-ATP synthase inhibitor that can induce p21(Cip1/Waf1) expression by induction of oxidative stress in human breast cancer cells. Cancer Res. 66 (9), 4880–4887.
Gootenberg, J.S., Abudayyeh, O.O., Kellner, M.J., Joung, J., Collins, J.J., Zhang, F., 2018. Multiplexed and portable nucleic acid detection platform with Cas13, Cas12a, and Csm6. Science 360 (6387), 439–444.
Harrington, L.B., Burstein, D., Chen, J.S., Paez-Espino, D., Ma, E., Witte, I.P., Cofsky, J.C., Kyrpides, N.C., Banfield, J.F., Doudna, J.A., 2018. Programmed DNA destruction by miniature CRISPR-Cas14 enzymes. Science 362 (6416), 839–842.
Hyman, A.A., Weber, C.A., Jülicher, F., 2014. Liquid-liquid phase separation in biology. Annu. Rev. Cell Dev. Biol. 30, 39–58.
Idzko, M., Ferrari, D., Eltzschig, H.K., 2014. Nucleotide signalling during inflammation. Nature 509 (7500), 310–317.
Imamura, H., Nhat, K.P., Togawa, H., Saito, K., Iino, R., Kato-Yamada, Y., Nagai, T., Noji, H., 2009. Visualization of ATP levels inside single living cells with fluorescence resonance energy transfer-based genetically encoded indicators. Proc. Natl. Acad. Sci. Unit. States Am. 106 (37), 15651–15656.
Jinek, M., Chylinski, K., Fonfara, I., Hauer, M., Doudna, J.A., Charpentier, E., 2012. A programmable Dual-RNA–guided DNA endonuclease in adaptive bacterial immunity. Science 337 (6096), 816–821.
Jo, S.-M., Wurm, F.R., Landfester, K., 2020. Oncolytic nanoreactors producing hydrogen peroxide for oxidative cancer therapy. Nano Lett. 20 (1), 526–533.
Kiekebusch, D., Thanbichler, M., 2014. Spatiotemporal organization of microbial cells by protein concentration gradients. Trends Microbiol. 22 (2), 65–73.
Lee, K.Y., Park, S.J., Lee, K.A., Kim, S.H., Kim, H., Meroz, Y., Mahadevan, L., Jung, K.H., Ahn, T.K., Parker, K.K., Shin, K., 2018. Photosynthetic artificial organelles sustain and control ATP-dependent reactions in a protocellular system. Nat. Biotechnol. 36 (6), 530–535.
Li, M., Qiao, S., Zheng, Y., Andaloussi, Y.H., Li, X., Zhang, Z., Li, A., Cheng, P., Ma, S., Chen, Y., 2020a. Fabricating covalent organic framework capsules with commodious microenvironment for enzymes. J. Am. Chem. Soc. 142 (14), 6675–6681.
Li, X., Pan, Y., Chen, C., Gao, Y., Liu, X., Yang, K., Luan, X., Zhou, D., Zeng, F., Han, X., Song, Y., 2021. Hypoxia-responsive gene editing to reduce tumor thermal tolerance for mild-photothermal therapy. Angew. Chem. Int. Ed. 60 (39), 21200–21204.
Li, X., Wang, X., Ito, A., Tsuji, N.M., 2020b. A nanoscale metal organic frameworks-based vaccine synergises with PD-1 blockade to potentiate anti-tumour immunity. Nat. Commun. 11 (1), 3858.
Liang, K., Ricco, R., Doherty, C.M., Styles, M.J., Bell, S., Kirby, N., Mudie, S., Haylock, D., Hill, A.J., Doonan, C.J., Falcaro, P., 2015. Biomimetic mineralization of metal-organic frameworks as protective coatings for biomacromolecules. Nat. Commun. 6 (1), 7240.
Lobas, M.A., Tao, R., Nagai, J., Kronschläger, M.T., Borden, P.M., Marvin, J.S., Looger, L. L., Khakh, B.S., 2019. A genetically encoded single-wavelength sensor for imaging cytosolic and cell surface ATP. Nat. Commun. 10 (1), 711.
Morciano, G., Sarti, A.C., Marchi, S., Missiroli, S., Falzoni, S., Raffaghello, L., Pistoia, V., Giorgi, C., Di Virgilio, F., Pinton, P., 2017. Use of luciferase probes to measure ATP in living cells and animals. Nat. Protoc. 12 (8), 1542–1562.
Pan, Y., Yang, J., Luan, X., Liu, X., Li, X., Yang, J., Huang, T., Sun, L., Wang, Y., Lin, Y., Song, Y., 2019. Near-infrared upconversion–activated CRISPR-Cas9 system: a remote-controlled gene editing platform. Sci. Adv. 5 (4), eaav7199.
Sun, Q., Fu, C.-W., Aguila, B., Perman, J., Wang, S., Huang, H.-Y., Xiao, F.-S., Ma, S., 2018. Pore environment control and enhanced performance of enzymes infiltrated in covalent organic frameworks. J. Am. Chem. Soc. 140 (3), 984–992.
Wang, Q., Liu, X., Zhou, J., Yang, C., Wang, G., Tan, Y., Wu, Y., Zhang, S., Yi, K., Kang, C., 2019. The CRISPR-Cas13a gene-editing system induces collateral cleavage of RNA in Glioma cells. Adv. Sci. 6 (20), 1901299.
Wu, X., Yue, H., Zhang, Y., Gao, X., Li, X., Wang, L., Cao, Y., Hou, M., An, H., Zhang, L., Li, S., Ma, J., Lin, H., Fu, Y., Gu, H., Lou, W., Wei, W., Zare, R.N., Ge, J., 2019. Packaging and delivering enzymes by amorphous metal-organic frameworks. Nat. Commun. 10 (1), 5165.
Xiong, Y., Zhang, J., Yang, Z., Mou, Q., Ma, Y., Xiong, Y., Lu, Y., 2020. Functional DNA regulated CRISPR-Cas12a sensors for point-of-care diagnostics of non-nucleic-acid targets. J. Am. Chem. Soc. 142 (1), 207–213.
Yang, X., Tang, Q., Jiang, Y., Zhang, M., Wang, M., Mao, L., 2019. Nanoscale ATP-responsive zeolitic imidazole framework-90 as a general platform for cytosolic protein delivery and genome editing. J. Am. Chem. Soc. 141 (9), 3782–3786.
Yu, Z., Zhou, P., Pan, W., Li, N., Tang, B., 2018. A biomimetic nanoreactor for synergistic chemiexcited photodynamic therapy and starvation therapy against tumor metastasis. Nat. Commun. 9 (1), 5044.
Zamaraeva, M.V., Sabirov, R.Z., Manabe, K., Okada, Y., 2007. Ca(2+)-dependent glycolysis activation mediates apoptotic ATP elevation in HeLa cells. Biochem. Biophys. Res. Commun. 363 (3), 687–693.
Zhang, C.-H., Wang, H., Liu, J.-W., Sheng, Y.-Y., Chen, J., Zhang, P., Jiang, J.-H., 2018a. Amplified split aptamer sensor delivered using block copolymer nanoparticles for small molecule imaging in living cells. ACS Sens. 3 (12), 2526–2531.
Zhang, L., Wang, Z., Zhang, Y., Cao, F., Dong, K., Ren, J., Qu, X., 2018b. Erythrocyte membrane cloaked metal–organic framework nanoparticle as biomimetic nanoreactor for starvation-activated colon cancer therapy. ACS Nano 12 (10), 10201–10211.
Zhao, D., Chang, D., Zhang, Q., Chang, Y., Liu, B., Sun, C., Li, Z., Dong, C., Liu, M., Li, Y., 2021a. Rapid and specific imaging of extracellular signaling molecule adenosine triphosphate with a self-phosphorylating DNAzyme. J. Am. Chem. Soc. 143 (37), 15084–15090.
Zhao, J., Gao, J., Xue, W., Di, Z., Xing, H., Lu, Y., Li, L., 2018. Upconversion Luminescence-activated DNA nanodevice for ATP sensing in living cells. J. Am. Chem. Soc. 140 (2), 578–581.
Zhao, Q., Pan, Y., Luan, X., Gao, Y., Zhao, X., Liu, Y., Wang, Y., Song, Y., 2021b. Nano-immunosorbent assay based on Cas12a/crRNA for ultra-sensitive protein detection. Biosens. Bioelectron. 190, 113450.
Zhou, T., Huang, R., Huang, M., Shen, J., Shan, Y., Xing, D., 2020. CRISPR/Cas13a powered portable electrochemiluminescence chip for ultrasensitive and specific MiRNA detection. Adv. Sci. 7 (13), 1903661.